Hydrothermal Synthesis and Characterization of Nitrogen-Doped Graphene from Puspa Wood Biomass

Muhammad Gibran Arrasyid[1,2*], Widayat Widayat[1,2], and Luqman Buchori[1]

[1]*Department of Chemical Engineering, Faculty of Engineering, Diponegoro University, Jl. Prof. Soedharto SH, Tembalang, Semarang 50275, Indonesia*

[2]*Advance Material Laboratory, Integrated Laboratory for Research and Services, Diponegoro University, Jl. Prof. Soedharto SH, Tembalang, Semarang 50275, Indonesia*

* ***Corresponding author:***

tel: +62-895423492620
email: gibranar1717@gmail.com

Received: November 29, 2025
Accepted: February 8, 2026

DOI: 10.22146/ijc.113615

Abstract: *The renewable energy transition demands efficient energy storage, where lithium-ion batteries (LiBs) are crucial for battery energy storage systems (BESS). This study reports the hydrothermal synthesis and characterization of nitrogen-doped graphene (NDG) from puspa wood biomass for anode applications. Puspa wood contains approximately 43.98% carbon with a low ash content of 1.256%, indicating its suitability as a carbon precursor. Through carbonization and graphitization, amorphous carbon was successfully transformed into an ordered graphite structure, as confirmed by the disappearance of –OH groups (3400–3600 cm^{-1}) in Fourier-transform infrared (FTIR) spectra and by X-ray diffraction (XRD) peak shifts from 23.50° to 26.50°. Subsequent oxidation produced graphene oxide (GO) characterized by carbonyl (C=O) groups at 1704 cm^{-1}, while nitrogen doping introduced C–N (1200 cm^{-1}) bonds, resulting in the formation of NDG. Nitrogen doping is known to enhance electrochemical properties. These findings highlight puspa wood as a promising precursor for NDG synthesis and provide a foundational material characterization that supports its further electrochemical investigation. This study demonstrates the promise of puspa wood biomass as a sustainable carbon source for advanced anode materials, contributing to eco-friendly battery technology.*

Keywords: *nitrogen-doped graphene; puspa wood biomass; lithium-ion battery; anode material; hydrothermal*

■ INTRODUCTION

The rising prices of conventional energy, combined with increasing energy demand and growing environmental concerns, are driving a shift toward sustainable renewable energy [1]. Hydropower was the largest source of global renewable energy capacity in 2021, totaling 1,362.087 GW out of a combined capacity of 3,089.984 GW. Solar photovoltaic energy followed with 866.027 GW, and wind energy contributed 825.663 GW [2]. This rapid growth highlights the promising future of renewable energy, inspiring confidence in its expanding role despite current challenges.

Battery energy storage systems (BESS) are vital for energy management, playing a crucial role in stabilizing and optimizing power systems. They help improve grid stability, make energy usage more efficient, and provide emergency power when needed [3]. Among the different rechargeable battery technologies available, lithium-ion batteries (LiBs) have become the most popular choice for BESS. This is because they offer several advantages, including high energy density, low self-discharge rates, long lifespan, lightweight design, and environmental compatibility [4-6]. As a result, LiBs are widely used in portable electronics, electric vehicles, and stationary energy storage systems [7].

LiBs have four main components: electrolyte, separator, cathode, and anode. The anode is particularly important because it affects the battery's performance by

managing the storage and release of lithium ions during discharge and charging [8]. Currently, graphite is the most commonly used anode material. However, it has some significant drawbacks, including a low theoretical specific capacity of 372 mAh/g, slow charging rates, and reduced performance at low temperatures [9]. Because of these issues, there has been a lot of research into alternative anode materials. These alternatives include alloy-based materials, transition-metal compounds, silicon-based materials, and advanced carbon-based materials, each with its own set of technical challenges [10].

Biomass-derived carbon materials are gaining popularity as sustainable alternatives for energy storage solutions. Puspa wood, in particular, stands out as a promising source of carbon with significant potential for advancing energy storage technologies, thanks to its high cellulose and hemicellulose content, favorable carbon-to-ash ratio, low sulfur content, and availability in many regions. By using controlled pyrolysis and carbonization methods, we can transform the complex molecular structure of puspa wood into ordered carbon frameworks, which are suitable for producing graphite and graphene. As shown in Table 1, puspa wood has a strong chemical composition compared to other common biomass sources like sugarcane bagasse, coconut shell, and rice husk. It offers higher carbon content and lower ash content, both of which are essential for creating high-purity carbon materials. Using puspa wood waste not only helps address environmental issues related to biomass disposal but also turns low-value waste into valuable carbon materials [11]. This study aims to investigate puspa wood as a new precursor for synthesizing nitrogen-doped graphene (NDG) and to assess its structural and chemical properties, supporting the development of innovative energy storage solutions.

Graphene is a fascinating material that has attracted significant attention due to its unique two-dimensional structure and impressive properties. It consists of a single layer of carbon atoms arranged in a hexagonal pattern [16-18]. This structure gives graphene remarkable strength, excellent electrical and thermal conductivity, and a large surface area [19]. These qualities make graphene a promising option for use in next-generation LiB anodes. Unlike conventional graphite, graphene-based anodes can store lithium ions on both sides of the sheet, potentially leading to a higher capacity [20]. However, one challenge with pure graphene is its tendency to clump, which can reduce its electrical conductivity and overall performance in electrochemical applications [18].

One effective way to address the limitations of graphene is through a process called heteroatom doping, with a focus on nitrogen doping. This technique can modify the electronic structure of graphene and improve its electrochemical properties. NDG can be created using several methods, such as chemical vapor deposition, solvothermal treatment, plasma processing, and hydrothermal synthesis. Among these options, the hydrothermal method stands out due to its simplicity, cost-effectiveness, scalability, and environmental friendliness. Incorporating nitrogen into the graphene structure introduces defects and micropores, which enhances the material's properties. This doping improves the wettability of the electrode, increases the energy with which ions bind to the surface, and allows for faster ion transport within the graphene framework [21-23].

There has been research on synthesizing NDG from various biomass sources, such as sugarcane bagasse and coconut shell, using techniques like high-temperature hydrothermal treatment and sonication. However, there hasn't been any reported research specifically on producing NDG from puspa wood biomass through a simple, moderate-temperature hydrothermal process [22,24-25]. Therefore, this study aims to develop an

Table 1. Chemical composition of biomass

Biomass sources	Cellulose (%)	Hemicellulose (%)	Lignin (%)	References
Puspa wood	51.20	16.60	27.00	[12]
Sugarcane bagasse	42.20	27.60	21.60	[13]
Coconut shell	30.58	26.70	33.30	[14]
Rice husk	35.00	25.00	20.00	[15]

eco-friendly and cost-effective hydrothermal method for synthesizing NDG from puspa wood biomass and to characterize its fundamental structural and chemical properties. The evaluation of these properties is essential to assess its potential suitability as a carbon-based anode material, which would require subsequent electrochemical validation in future work. By utilizing a renewable biomass precursor, this work contributes to the development of sustainable carbon materials while reducing dependence on fossil-based resources [18].

■ EXPERIMENTAL SECTION

Materials

Puspa wood biomass was obtained from a local market in Indonesia. The chemicals used in this study included sodium nitrate ($NaNO_3$, Merck), concentrated sulfuric acid (H_2SO_4, Merck), potassium permanganate ($KMnO_4$, Merck), hydrogen peroxide (H_2O_2, Merck), and hydrochloric acid (HCl, Merck), all of analytical grade. Deionized water and distilled water were also used. All materials were used without further purification.

Instrumentation

The biomass was processed using a laboratory saw, grinder, and digital balance (Ohaus). Drying was conducted in a laboratory oven, and particle size reduction was performed using a sieve shaker equipped with a 200-mesh sieve. Carbonization and ashing were performed in a Thermolyne muffle furnace, while high-temperature graphitization was carried out using a Nabertherm RHTH 120/600 high-temperature vacuum furnace (1800 °C). Sample preparation utilized a magnetic stirrer, hot plate, vacuum pump, ice bath, thermometer, glassware, and filter paper. Exfoliation and dispersion processes employed a BIOBASE Ultrasonic Cell Disrupter UCD-1000 probe sonicator. Elemental composition (CHNS) was analyzed using a CHNS Elementar analyzer. Crystalline structure was examined with a Shimadzu XRD-7000 diffractometer, while functional groups were identified using a Perkin-Elmer UATR Spectrum Two instrument.

Procedure

Puspa wood powder was oven-dried at 105 °C for 2 h and sieved to obtain particles smaller than 1 mm [26]. Moisture and ash contents were determined following ASTM E871-80 and ASTM E1755, with the ashing conducted in a Thermolyne muffle furnace. Ultimate analysis for CHNS was performed using a Perkin-Elmer 2004 instrument. The dried biomass was carbonized at 600 °C for 3 h in a Nabertherm vacuum furnace, and the resulting char was subsequently graphitized at 1300 °C to convert amorphous carbon into crystalline graphite [27-28]. The graphitized material was crushed, sieved to 0.074 mm, and purified by stirring in 0.5 M HCl (1:10 w/v) for 12 h at room temperature to remove metal impurities. The purified graphite was rinsed to neutral pH and dried at 105 °C for 3 h.

Graphite oxide (GrO) was synthesized from purified graphite using a modified Hummers method. 1 g of graphite was mixed with 0.5 g of $NaNO_3$ in 25 mL of conc. H_2SO_4 and stirred in an ice bath for 30 min to maintain the temperature below 20 °C. $KMnO_4$ (3 g) was then added gradually under the same conditions, followed by stirring for 3 h until a dark-green color indicated successful oxidation. Subsequently, 50 mL of deionized water was added slowly, and the mixture was heated to 90 °C. After cooling to 40–60 °C, 100 mL of deionized water and 5 mL of H_2O_2 were added to terminate the reaction. The resulting GrO was allowed to stand overnight, filtered, washed to neutral pH, and dried at 50 °C [27,29-30].

The obtained GrO was used as the starting material for NDG synthesis. For this purpose, 10 mg of GrO was dispersed in 60 mL of deionized water and sonicated for 1 h to exfoliate it into graphene oxide (GO) sheets and to ensure a homogeneous suspension. Then, 1 g of urea was added as a nitrogen source, and the mixture was stirred at 300 rpm for 20 min. The suspension was transferred into a 200 mL Teflon-lined autoclave and subjected to hydrothermal treatment at 120 °C for 12 h. After cooling to room temperature, the resulting product was washed with distilled water and dried at 60 °C for 12 h to obtain NDG [31]. Characterization was conducted at different stages, including moisture and ash determinations, elemental composition, XRD, and FTIR analyses.

■ RESULTS AND DISCUSSION

The properties of puspa wood powder were analyzed through ultimate analysis, as well as moisture and ash content tests, as summarized in Table 2. The ultimate analysis revealed that the elemental composition of puspa wood consists of 43.98% carbon (C), 7.408% hydrogen (H), 0.27% nitrogen (N), 0.045% sulfur (S), and 48.297% oxygen (O, calculated by difference). The moisture content and ash content of puspa wood powder were found to be 10.596 and 1.256%, respectively. To evaluate the suitability of puspa wood as a carbon precursor, these values were compared with other biomass sources such as sugarcane bagasse, coconut shell, rice husk, and oil palm shell, also presented in Table 3. In comparison, the carbon content of puspa wood (43.98%) is higher than that of bagasse (43.38%) and rice husk (35.8%), but slightly lower than that of coconut shell (47.17%) and oil palm shell (48.68%). The hydrogen content of puspa wood (7.408%) is higher than in all other referenced biomasses, indicating a higher volatile matter content. Nitrogen and sulfur levels were low (0.27 and 0.045%, respectively), comparable to other biomasses, which is beneficial for minimizing pollutant emissions during carbonization.

Related to moisture content, puspa wood (10.596%) falls between the values of sugarcane bagasse (7.95%) and rice husk (9.5%) on the lower end, and coconut shell (12%) and oil palm shell (15.21%) on the higher end, suggesting that pre-drying could enhance carbonization efficiency. The ash content of puspa wood (1.256%) is significantly lower than that of rice husk (16.3%) and oil palm shell (7.75%), and slightly higher than that of bagasse (1%) but notably lower than coconut shell (3.4%). This low ash content indicates that puspa wood generates minimal inorganic residue post-carbonization, reinforcing its potential as a high-purity carbon source [32-35].

FTIR was used to identify the functional groups present in puspa wood charcoal, puspa wood graphite, GrO, GO, and NDG. Fig. 1 shows the spectra of puspa wood charcoal and puspa wood graphite. The charcoal spectrum exhibits absorption in the range of 3400–3600 cm^{-1}, indicating the presence of –OH groups. This suggests the decomposition of cellulose, hemicellulose, and lignin constituents. In contrast, the graphite spectrum shows no absorption in this region, confirming that graphitization has led to the complete elimination of –OH groups through the total decomposition of biomass components [36-39]. Charcoal displays a distinct absorption peak at 1693 cm^{-1}, corresponding to C=O bonds from acetyl ester and/or aldehyde functional groups, which are residues of hemicellulose and lignin. The peak at 1577 cm^{-1} indicates the presence of C=C bonds, suggesting the onset of graphitization as a result of localized carbon structures [36,40]. An additional absorption peak at 1405 cm^{-1} represents C–H bonds, likely originating from lignin components that were not fully decomposed [41]. The band at 1169 cm^{-1} is attributed to C–O–C groups [42], while the absorption at 858 cm^{-1}

Table 2. Properties of sawdust used in this study

Properties	wt.%
Moisture content	10.596
Ash content	1.256
Ultimate analysis	
C	43.980
H	7.408
N	0.270
S	0.045
O*	48.297

*Calculated from the difference

Table 3. Comparison properties of puspa wood with other biomass

Biomass sources	C (%)	H (%)	N (%)	S (%)	O (%)*	Moisture (%)	Ash (%)	References
Puspa wood	43.98	7.408	0.27	0.045	48.297	10.596	1.256	This study
Sugarcane bagasse	43.38	6.13	0.20	0.05	50.24	7.95	1.00	[32]
Coconut shell	47.17	6.50	0.21	0.04	46.08	12.00	3.40	[33]
Rice husk	35.80	5.80	0.25	0.06	58.09	9.50	16.30	[34]
Oil palm shell	48.68	6.16	0.22	0.05	44.89	15.21	7.75	[35]

*Calculated from the difference

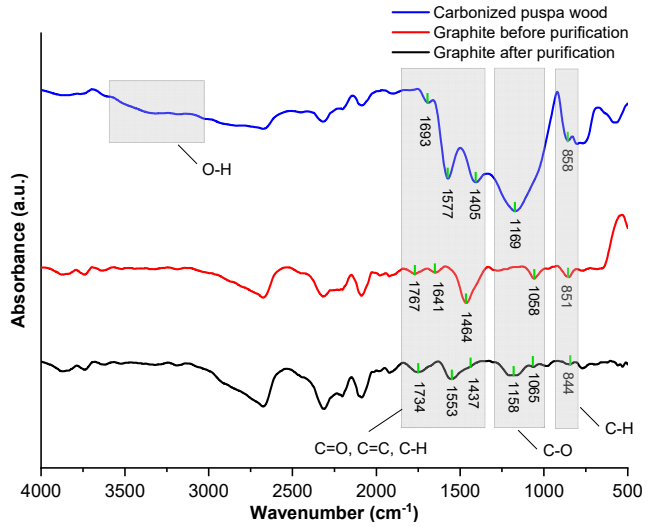

Fig 1. FTIR spectra of charcoal, graphite before and after washing

indicates the presence of aromatic C–H bonds, signifying that some aromatic ring structures were retained. This is typical in carbon materials like graphite. However, while FTIR can effectively identify functional groups, it does not provide sufficient information about layer thickness or the degree of graphene exfoliation [43].

In contrast to charcoal, the absorption bands observed in graphite exhibit variations in intensity, although the functional groups remain interconnected. As shown in Fig. 1, the absence of absorption in the 3400–3600 cm^{-1} region indicates that –OH groups are no longer present in graphite. This confirms that the graphitization process was successful in eliminating –OH functionalities, signaling the complete decomposition of cellulose, hemicellulose, and lignin [44]. The C=O peaks in graphite—both before and after washing—appear less intense than in charcoal, with peaks observed at 1767 cm^{-1} (before washing) and 1734 cm^{-1} (after washing). This suggests a reduction in C=O groups following further purification [45]. Furthermore, the peaks at 1641 and 1553 cm^{-1} in graphite are more symmetrical than those in charcoal, indicating a more orderly and homogeneous distribution of C=C bonds [40]. The peaks at 1464 and 1437 cm^{-1} also show reduced intensity, especially in washed graphite, reflecting a more complete decomposition of lignin components [41,46]. A clear difference is observed between graphite before and after washing. In unwashed graphite, a single absorption peak appears at 1058 cm^{-1}, corresponding to C–O stretching in alkoxy groups [47]. In contrast, the washed graphite shows two distinct peaks at 1158 and 1065 cm^{-1}, which are attributed to C–O–C and C–O groups, respectively [48-49]. Lastly, absorption bands at 851 cm^{-1} (before washing) and 844 cm^{-1} (after washing) correspond to aromatic C–H bonds, whose reduced intensity compared to charcoal indicates a higher degree of graphitization and improved graphite quality [41,43].

Fig. 2 shows that the FTIR spectra of GrO and GO exhibit similar patterns, with no significant structural changes observed. This is expected, as GO is essentially

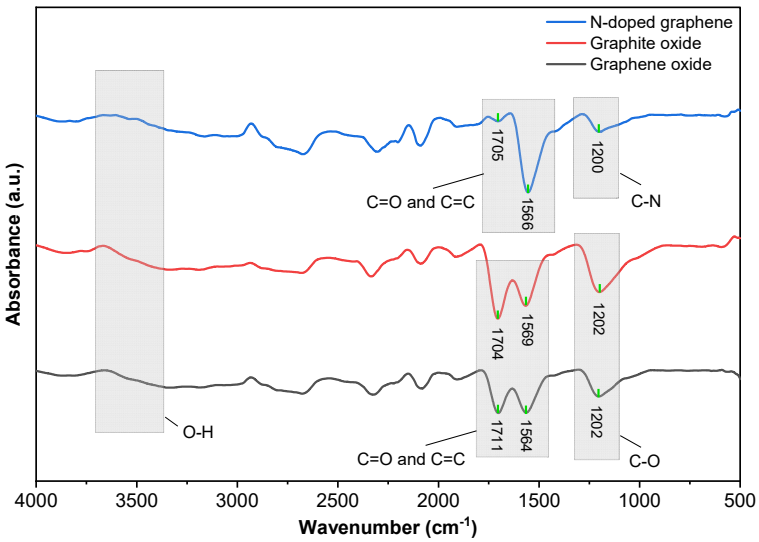

Fig 2. FTIR spectra of GrO, GO, and NDG

a more exfoliated form of GrO, produced through sonication. In the range of 3400–3600 cm^{-1}, a broad absorption band corresponding to –OH stretching is observed in both samples, confirming the presence of –OH and indicating successful synthesis using the modified Hummers method [30]. The peaks at 1704 cm^{-1} (GrO) and 1711 cm^{-1} (GO) correspond to C=O stretching vibrations, which are characteristic of oxidized graphite structures and are a direct result of the oxidation process introduced by the modified Hummers method [27,50-51]. Meanwhile, the bands at 1569 cm^{-1} for GrO and 1564 cm^{-1} for GO are attributed to unoxidized C=C bonds remaining within the graphitic domains, indicating partial retention of the original sp^2-hybridized carbon structure [52-53]. Both spectra also show a peak at 1202 cm^{-1}, associated with the C–O–C group, likely originating from cellulose-based residues in the original graphite precursor [36,49].

In contrast, the FTIR spectrum of NDG reveals the emergence of three key functional groups consistent with nitrogen doping: C=C and C–N bonds [54-55]. The persistence of the C=C bond absorption at 1566 cm^{-1} indicates that the doping process does not completely disrupt the carbon network, allowing the retention of the underlying sp^2-hybridized structure [56]. A new peak at 1200 cm^{-1} is attributed to C–N stretching, which results from the reduction of oxygen-containing groups (e.g., C–O) and their substitution by nitrogen functionalities. This transformation suggests the effective substitution of C–O groups in GO by C–N groups in NDG [53,55]. It is important to note that while FTIR effectively identifies functional groups present in the samples, it does not provide sufficient information regarding the layer thickness or the degree of exfoliation of graphene materials.

The successful nitrogen doping of biomass-derived graphene has been achieved via various methods, as summarized in Table 4. For example, NDG has been synthesized from sugarcane bagasse using high-temperature hydrothermal treatment and from coconut shell via sonication or ammonia treatment [21,24-25]. In this work, we demonstrate that a moderate hydrothermal process (120 °C, 12 h) with urea is equally effective for doping nitrogen into graphene derived from the novel puspa wood precursor, as confirmed by the characteristic C–N (1200 cm^{-1}) FTIR peaks. This consistency across different biomass sources and doping techniques validates the core finding of successful NDG synthesis and situates our methodological approach within the existing literature.

Fig. 3 displays XRD patterns of carbonized charcoal and graphite, both before and after the washing process. The presence of amorphous phases in the samples may be attributed to the use of biomass-based raw materials [27]. The diffractogram data were analyzed using X'Pert HighScore Plus software to identify the crystalline phases and elemental compositions. For reference from JCPDS 00-041-1487, pure graphite typically exhibits a characteristic diffraction peak at $2\theta = 26.54°$. In contrast, the diffractogram of puspa wood charcoal indicates that the carbon remains predominantly in an amorphous form. A notable peak at $2\theta = 29.82°$ suggests the presence of inorganic mineral content, specifically calcium carbonate ($CaCO_3$), which is

Table 4. Comparison of synthesis methods and FTIR of NDG from various biomass precursors

Biomass precursor	Nitrogen sources/doping methods	FTIR peaks (cm^{-1})	Study focus	References
Puspa wood	Urea/Hydrothermal (120 °C, 12 h)	C–N: 1200	Synthesis and characterization for LiB anode potential	This study
Sugarcane bagasse	Urea/Hydrothermal (240 °C, 24 h)	C=N: ~1550, C–N: ~1197	Synthesis for supercapacitor electrode	[22]
Coconut shell	Urea/Mechanical sonication (6 h)	C≡N ~2400, C–N: ~1150	Synthesis of working electrodes	[24]
Coconut shell	Ammonia (NH_3)/Stirring (72 h, r.t.)	C–N: 1396	Synthesis for electrical conductivity measurement	[25]

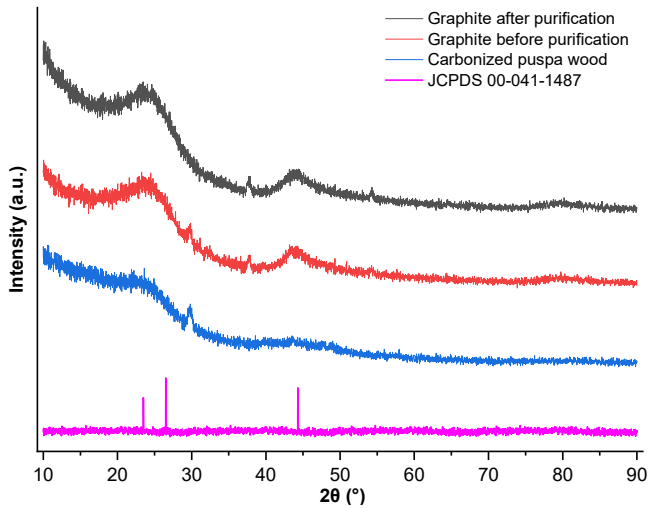

Fig 3. XRD profile of charcoal, graphite before washing, graphite after washing

often retained from the biomass source [10]. The XRD patterns of graphite, both before and after washing, exhibit a sharp peak within the 2θ range of 23.50°–26.50°, indicating a more ordered crystalline structure compared to the amorphous charcoal [30]. Additionally, a distinct peak observed around 2θ = 43.00°–44.00° further supports the improved graphitic ordering in these samples [27].

Another diffraction peak observed at 2θ = 37.70° may be attributed to a reaction between the carbon sample and the alumina (Al_2O_3) crucible at high temperatures during graphitization [57-58]. Washing treatment using HCl appears effective in removing residual $CaCO_3$, as evidenced by the absence of corresponding peaks in the washed graphite sample. This suggests that the post-washing graphite exhibits higher purity compared to the unwashed version. In summary, the XRD analysis confirms the successful transformation of amorphous charcoal into a more crystalline graphite structure, with HCl washing further enhancing the purity by eliminating inorganic contaminants such as $CaCO_3$.

This study has several limitations that point to needed future work. First, the electrochemical performance of the synthesized NDG as a LiB anode has not been tested. Data from cyclic voltammetry, galvanostatic charge–discharge, and impedance spectroscopy are required to confirm its battery potential. Furthermore, material characterization relied primarily on FTIR and XRD, which lack the depth provided by complementary techniques such as Raman spectroscopy (for defect analysis), electron microscopy (for morphology), surface area analysis (BET), and XPS (for nitrogen bonding configuration). Because of these limitations, a direct quantitative comparison with other NDG materials was not possible. Future studies should therefore focus on both electrochemical testing and deeper material analysis to fully assess NDG's suitability for energy storage.

■ CONCLUSION

NDG was successfully synthesized from puspa wood biomass through a multi-step process involving carbonization, graphitization, oxidation, and a moderate-temperature hydrothermal doping using urea. FTIR analysis confirmed the incorporation of nitrogen via the presence of characteristic C–N bonds, while XRD indicated the transformation of amorphous carbon into a more ordered graphitic structure. These findings establish puspa wood as a viable and novel precursor for sustainable carbon materials. However, the definitive assessment of its electrochemical performance as a LiB anode remains beyond the scope of this foundational work and constitutes its primary limitation. Therefore, while the synthesized NDG exhibits promising structural properties, future research must include comprehensive electrochemical characterization (e.g., CV, EIS, galvanostatic) alongside advanced material analysis (e.g., Raman, BET, XPS) to validate its practical utility in energy storage applications.

■ ACKNOWLEDGMENTS

The authors gratefully acknowledge the financial support from LPPM Diponegoro University for this research with contract number 222-557/UN7.D2/PP/IV/2025.

■ CONFLICT OF INTEREST

The authors declare no conflict of interest.

■ AUTHOR CONTRIBUTIONS

Muhammad Gibran Arrasyid conducted the experiment, performed the calculations, and wrote the manuscript. Widayat and Luqman Buchori checked and

revised the manuscript. All authors agreed to the final version of this manuscript.

■ REFERENCES

[1] Wei, P., Abid, M., Adun, H., Kemena Awoh, D., Cai, D., Zaini, J.H., and Bamisile, O., 2023, Progress in energy storage technologies and methods for renewable energy systems application, *Appl. Sci.*, 13 (9), 5626.

[2] IRENA, 2023, *Renewable energy statistics 2023*, International Renewable Energy Agency, Abu Dhabi.

[3] Conzen, J., Lakshmipathy, S., Kapahi, A., Kraft, S., and DiDomizio, M., 2023, Lithium ion battery energy storage systems (BESS) hazards, *J. Loss Prev. Process Ind.*, 81, 104932.

[4] Writer, B., 2019, *Lithium-Ion Batteries*, Springer International Publishing, Cham, Switzerland.

[5] Asghar, M.R., Anwar, M.T., Rasheed, T., Naveed, A., Yan, X., and Zhang, J., 2019, Lithium salt doped poly(vinylidene fluoride)/cellulose acetate composite gel electrolyte membrane for lithium ion battery, *IOP Conf. Ser.: Mater. Sci.*, 654 (1), 012017.

[6] Jyoti, J., Singh, B.P., and Tripathi, S.K., 2021, Recent advancements in development of different cathode materials for rechargeable lithium-ion batteries, *J. Energy Storage*, 43, 103112.

[7] Cheng, X.B., Zhang, R., Zhao, C.Z., Wei, F., Zhang, J.G., and Zhang, Q., 2016, A review of solid electrolyte interphases on lithium metal anode, *Adv. Sci.*, 3 (3), 1500213.

[8] Al Ja'farawy, M.S., Hikmah, D.N., Riyadi, U., Purwanto, A., and Widiyandari, H., 2021, A review: The development of SiO_2/C anode materials for lithium-ion batteries, *J. Electron. Mater.*, 50 (12), 6667–6687.

[9] Hossain, M.H., Chowdhury, M.A., Hossain, N., Islam, M.A., and Mobarak, M.H., 2023, Advances of lithium-ion batteries anode materials—A review, *Chem. Eng. J. Adv.*, 16, 100569.

[10] Nzereogu, P.U., Omah, A.D., Ezema, F.I., Iwuoha, E.I., and Nwanya, A.C., 2022, Anode materials for lithium-ion batteries: A review, *Appl. Surf. Sci. Adv.*, 9, 100233.

[11] Asri, W.R., Mara, A., Desnelli, D., and Hasanudin, H., 2022, Pyrolysis of puspa wood sawdust and sugarcane bagasse into biochar, *Aceh Int. J. Sci. Technol.*, 11 (1), 56–69.

[12] Syahri, T.N., 1988, Analisis kimia 75 jenis kayu dari beberapa lokasi di Indonesia, *Jurnal Penelitian Hasil Hutan*, 5 (1), 6–11.

[13] Nunes, L.J.R., Loureiro, L.M.E.F., Sá, L.C.R., and Silva, H.F.C., 2020, Sugarcane industry waste recovery: A case study using thermochemical conversion technologies to increase sustainability, *Appl. Sci.*, 10 (18), 6481.

[14] Arena, N., Lee, J., and Clift, R., 2016, Life cycle assessment of activated carbon production from coconut shells, *J. Cleaner Prod.*, 125, 68–77.

[15] Saiful Islam, M., Jamal, M.S., Sujan, S.M.A., Ismail, M., Yunus Miah, M., and Saha, M., 2011, Bio-oil from pyrolysis of rice husk, *J. Biofuel*, 2 (1), 1–7.

[16] Novoselov, K.S., Geim, A.K., Morozov, S.V., Jiang, D., Zhang, Y., Dubonos, S.V., Grigorieva, I.V., and Firsov, A.A., 2004, Electric field effect in atomically thin carbon films, *Science*, 306 (5696), 666–669.

[17] Okhay, O., and Tkach, A., 2024, A comprehensive review of the use of porous graphene frameworks for various types of rechargeable lithium batteries, *J. Energy Storage*, 80, 110336.

[18] Zare, Y., Kim, T.H., Gharib, N., and Chang, Y.W., 2023, Effect of contact number among graphene nanosheets on the conductivities of tunnels and polymer composites, *Sci. Rep.*, 13 (1), 9506.

[19] Xu, H., Ma, L., and Jin, Z., 2018, Nitrogen-doped graphene: Synthesis, characterizations and energy applications, *J. Energy Chem.*, 27 (1), 146–160.

[20] Lang, J., Zhang, X., Liu, B., Wang, R., Chen, J., and Yan, X., 2018, The roles of graphene in advanced Li-ion hybrid supercapacitors, *J. Energy Chem.*, 27 (1), 43–56.

[21] Das, T.K., Banerjee, S., Kumar, A., Debnath, A.K., and Sudarsan, V., 2019, Electrochemical performance of hydrothermally synthesized N-doped reduced graphene oxide electrodes for supercapacitor application, *Solid State Sci.*, 96, 105952.

[22] Ye, W., Cai, J., Yu, F., Li, X., and Wang, X., 2021, Nitrogen-doped bagasse carbon spheres/graphene composite for high-performance supercapacitors, *Biomass Bioenergy*, 145, 105949.

[23] Wang, X., and Shi, G., 2015, An introduction to the chemistry of graphene, *Phys. Chem. Chem. Phys.*, 17 (43), 28484–28504.

[24] Khambali, I., Priyanto, B., Asih, R., Baqiya, M.A., Ramli, M.M., Osman, N.H., Tunmee, S., Nakajima, H., Triwikantoro, T., Zainuri, M., and Darminto, D., 2022, N-doped rGO-like carbon prepared from coconut shell: Structure and specific capacitance, *J. Renewable Mater.*, 11 (4), 1823–1833.

[25] Supeno, M., Pratama, A., and Haulian Purba, R., 2020, Adsorption of N-graphene from coconut shell, *Orient. J. Chem.*, 36 (2), 280–285.

[26] Varma, A.K., and Mondal, P., 2016, Physicochemical characterization and pyrolysis kinetic study of sugarcane bagasse using thermogravimetric analysis, *J. Energy Resour. Technol.*, 138 (5), 052205.

[27] Sujiono, E.H., Zurnansyah, Z., Zabrian, D., Dahlan, M.Y., Amin, B.D., Samnur, S., and Agus, J., 2020, Graphene oxide based coconut shell waste: Synthesis by modified Hummers method and characterization, *Heliyon*, 6 (8), e04568.

[28] Gutiérrez-Pardo, A., Ramírez-Rico, J., Cabezas-Rodríguez, R., and Martínez-Fernández, J., 2015, Effect of catalytic graphitization on the electrochemical behavior of wood derived carbons for use in supercapacitors, *J. Power Sources*, 278, 18–26.

[29] Darmawan, A., Listanti, D.A., Muhtar, H., Azmiyawati, C., and Bima, D.N., 2025, Innovative structured brick-and-mortar graphene oxide/polyvinyl pyrrolidone composite membrane for highly efficient desalination via pervaporation, *Colloids Surf., A*, 707, 135853.

[30] Ariyanti, D., Lesdantina, D., Purbasari, A., and Astuti, Y., 2023, Synthesis of graphene-like material derived from biomass from agricultural waste and its application in Cu(II) removal, *Korean J. Chem. Eng.*, 40 (4), 964–974.

[31] Dong, J., Lu, G., Wu, F., Xu, C., Kang, X., and Cheng, Z., 2018, Facile synthesis of a nitrogen-doped graphene flower-like MnO_2 nanocomposite and its application in supercapacitors, *Appl. Surf. Sci.*, 427, 986–993.

[32] Parmar, P., Mukherjee, S., Kumar Singh, V., and Meikap, B.C., 2024, Thermo-kinetic analysis of sugarcane bagasse as a sustainable energy resource evaluation, *Therm. Sci. Eng. Prog.*, 54, 102836.

[33] George, J., Arun, P., and Muraleedharan, C., 2017, Effect of operating parameters in air-steam gasification, *J. Adv. Eng. Res.*, 4 (2), 89–93.

[34] Vaskalis, I., Skoulou, V., Stavropoulos, G., and Zabaniotou, A., 2019, Towards circular economy solutions for the management of rice processing residues to bioenergy via gasification, *Sustainability*, 11 (22), 6433.

[35] Waluyo, J., Makertihartha, I.G.B.N., and Susanto, H., 2018, Pyrolysis with intermediate heating rate of palm kernel shells: Effect temperature and catalyst on product distribution, *AIP Conf. Proc.*, 1977 (1), 020026.

[36] Mohamed, K.M., Vijaya, J.J., Paul Winston, A.J.P., Akash, K., Sagayaraj, P., Rajeshkumar, S., and Al-Sadoon, M.K., 2024, Untapped potential: Sugarcane bagasse to biocompatible graphene oxide as biomedicine, *Diamond Relat. Mater.*, 148, 111479.

[37] Azahar, A.A., Nurhafizah, M.D., Omar, M.R., Abdullah, N., and Ul-Hamid, A., 2022, Bio-graphene production from oil palm shell waste valorised through sequential thermal and catalytic means, *Carbon Trends*, 9, 100225.

[38] Sarkar, J.K., and Wang, Q., 2020, Different pyrolysis process conditions of South Asian waste coconut shell and characterization of gas, bio-char, and bio-oil, *Energies*, 13 (8), 1970.

[39] Barakat, N.A.M., Gamal, S., Abdul Hameed, M.M., Fadali, O.A., Abdelraheem, O.H., Hefny, R.A., and Moustafa, H.M., 2023, Graphitized corncob 3D Biomass-driven anode for high performance batch and continuous modes air-cathode microbial fuel cells working by domestic wastewater, *Int. J. Hydrogen Energy*, 48 (98), 38854–38869.

[40] Mahmun, A., and Deoghare, A.B., 2024, A comparative study on coconut shell-derived

graphene oxide and reduced graphene oxide, *Curr. Appl Phys.*, 62, 12–21.

[41] Nanda, S., Mohanty, P., Pant, K.K., Naik, S., Kozinski, J.A., and Dalai, A.K., 2013, Characterization of North American lignocellulosic biomass and biochars in terms of their candidacy for alternate renewable fuels, *Bioenergy Res.*, 6 (2), 663–677.

[42] Pan, N., Guan, D., He, T., Wang, R., Wyman, I., Jin, Y., and Xia, C., 2013, Removal of Th^{4+} ions from aqueous solutions by graphene oxide, *J. Radioanal. Nucl. Chem.*, 298 (3), 1999–2008.

[43] Rampe, M.J., Santoso, I.R.S., Rampe, H.L., Tiwow, V.A., and Rorano, T.E.A., 2022, Study of pore length and chemical composition of charcoal that results from the pyrolysis of coconut shell in Bolaang Mongondow, Sulawesi, Indonesia, *Karbala Int. J. Mod. Sci.*, 8 (1), 96–104.

[44] Guye, M.E., Dabaro, M.D., and Kim, H., 2025, Biomass-derived graphitic-like hierarchical porous carbon for electrochemical supercapacitor application, *J. Energy Storage*, 115, 116037.

[45] Singh, S.B., and De, M., 2020, Thermally exfoliated graphene oxide for hydrogen storage, *Mater. Chem. Phys.*, 239, 122102.

[46] Silverstein, R.M., Webster, F.X., and Kiemle, D.J., 2005, *Spectrometric Identification of Organic Compound*, Wiley, Hoboken, New Jersey, US.

[47] Bera, M., Chandravati, C., Gupta, P., and Maji, P.K., 2017, Facile one-pot synthesis of graphene oxide by sonication assisted mechanochemical approach and its surface chemistry, *J. Nanosci. Nanotechnol.*, 18 (2), 902–912.

[48] Platnieks, O., Gaidukovs, S., Barkane, A., Sereda, A., Gaidukova, G., Grase, L., Thakur, V.K., Filipova, I., Fridrihsone, V., Skute, M., and Laka, M., 2020, Bio-based poly(butylene succinate)/microcrystalline cellulose/nanofibrillated cellulose-based sustainable polymer composites: Thermo-mechanical and biodegradation studies, *Polymers*, 12 (7), 1472.

[49] Ossonon, B.D., and Bélanger, D., 2017, Synthesis and characterization of sulfophenyl-functionalized reduced graphene oxide sheets, *RSC Adv.*, 7 (44), 27224–27234.

[50] Yu, H., Zhang, B., Bulin, C., Li, R., and Xing, R., 2016, High-efficient synthesis of graphene oxide based on improved Hummers method, *Sci. Rep.*, 6 (1), 36143.

[51] Husain, H., Ramli, I., Adi, W.A., Yunasfi, Y., Mashadi, M., Mulyawan, A., Winatapura, D.S., Subaer, S., Taryana, Y., Wahyu, Y., Dewi, N., and Susanto, A., 2025, Sustainable synthesis and structural characterization of carbon, graphite, graphene oxide, and reduced graphene oxide derived from coconut shells, *Indones. J. Chem.*, 25 (6), 1768–1777.

[52] Emiru, T.F., and Ayele, D.W., 2017, Controlled synthesis, characterization and reduction of graphene oxide: A convenient method for large scale production, *Egypt. J. Basic Appl. Sci.*, 4 (1), 74–79.

[53] Guo, H.L., Wang, X.F., Qian, Q.Y., Wang, F.B., and Xia, X.H., 2009, A green approach to the synthesis of graphene nanosheets, *ACS Nano*, 3 (9), 2653–2659.

[54] Jayabal, E., Natarajan, A., and Rengarajan, V., 2021, One-pot hydrothermal synthesis of nitrogen-doped reduced graphene oxide for the highly sensitive and simultaneous determination of dihydroxy benzene isomers, *J. Appl. Electrochem.*, 51 (8), 1189–1205.

[55] Ajravat, K., Rajput, S., and Brar, L.K., 2022, Microwave assisted hydrothermal synthesis of N doped graphene for supercapacitor applications, *Diamond Relat. Mater.*, 129, 109373.

[56] Kumar, M.P., Kesavan, T., Kalita, G., Ragupathy, P., Narayanan, T.N., and Pattanayak, D.K., 2014, On the large capacitance of nitrogen doped graphene derived by a facile route, *RSC Adv.*, 4 (73), 38689–38697.

[57] Mohammed, A.A., Khodair, Z.T., and Khadom, A.A., 2020, Preparation and investigation of the structural properties of α-Al_2O_3 nanoparticles using the sol-gel method, *Chem. Data Collect.*, 29, 100531.

[58] Hameed, M.A., and Ahmed, L.M., 2024, SDS-Assisted hydrothermal growth and photocatalytic activity of like-caviar $MoFe_2O_4$ nanoparticle decorated with Al_2O_3, *Indones. J. Chem.*, 24 (3), 776–790.